

# Preparation and Characterization of Thermally Stable Phosphonium Organoclays and Their Use in Poly(ethylene terephthalate) Nanocomposites

Wissam Abdallah, Ulku Yilmazer

Department of Chemical Engineering, Middle East Technical University, 06800 Ankara, Turkey

Correspondence to: U. Yilmazer (E-mail: yilmazer@metu.edu.tr)

**ABSTRACT:** Purification of montmorillonite rich bentonite followed by surface modification using organic salts was performed. The bentonite was purified by sedimentation and then surface modified by ion exchange using alkyl- and aryl-based phosphonium salts. The thermal stability, morphology, melt flow, and mechanical properties of the poly(ethylene terephthalate) (PET) nanocomposites prepared with these organoclays were studied with and without using a reactive elastomeric compatibilizer. TEM results showed that the alkyl based organoclay exhibited better dispersion and thus, higher tensile strength and elongation at break in the PET/organoclay/elastomer ternary nanocomposites than the aryl-based organoclay did. The notched Charpy impact strength of PET increased from 2.9 to 4.7 kJ m<sup>-2</sup> and 3.4 kJ m<sup>-2</sup> for alkyl and aryl phosphonium organoclay-based ternary nanocomposites, respectively. Upon compounding PET with alkyl and aryl phosphonium organoclays, the onset decomposition temperature of PET increased from 413°C to 420°C and 424°C, respectively. © 2012 Wiley Periodicals, Inc. *J. Appl. Polym. Sci.* 128: 4283–4293, 2013

**KEYWORDS:** clay; mechanical properties; polyesters; properties and characterization; thermogravimetric analysis (TGA)

Received 29 May 2012; accepted 28 September 2012; published online 22 October 2012

**DOI:** 10.1002/app.38651

## INTRODUCTION

Nanocomposites constitute one of the most recent areas of nanotechnology. Polymer–clay nanocomposites, specifically, have perceived great augment in the past decade. The smart characteristics of polymer–clay nanocomposites suggest a variety of potential industrial uses: automotive, construction, aerospace, food packaging, textiles, etc.<sup>1</sup> Upon loading of few percentages of clay, the nanocomposite may possess various enhanced properties that attract a wide range of different industrial applications. The diversity of structures and properties of clays and clay minerals and their vast ranging applications made them highly prominent for the industry.<sup>2–4</sup>

Bentonite clays have a broad scope of application domains before and after processing. Most clay minerals are found together with other minerals and/or amorphous materials. The increasing applications of clay minerals in the manufacture of advanced materials raised the need for enrichment by purification.<sup>5</sup> Because smectites are the major minerals in bentonites, the isolation of smectite group minerals from bentonites is of great importance. The presence of impurities severely affects the cation exchange capacity, and mechanical, thermal and optical properties of polymer based nanocomposites prepared by these bentonites.<sup>6</sup>

Montmorillonite (MMT) is the most common mineral of the smectite group.<sup>7</sup> Among the diverse types of layered silicates, MMT is particularly attractive as reinforcement for polymer–clay nanocomposites by virtue of its high platelet aspect ratio, morphology, natural abundance, ecological nature, and low cost.<sup>1,8</sup> It is a naturally occurring 2:1 phyllosilicate with a high surface area of ~750 m<sup>2</sup> g<sup>-1</sup>, and its crystal lattice is composed of two silica tetrahedral sheets (SiO<sub>4</sub>) and an octahedral alumina sheet (AlO<sub>4</sub>(OH)<sub>4</sub>) between the tetrahedrons.<sup>9</sup>

The conventional hydrophilic silicate surface becomes organophilic after the ion exchange process of hydrated ions present in layered silicates with cationic surfactants. As a result, the surface energy of MMT decreases, the wetting properties of polymer–clay interface gets enhanced, and the basal spacing expands causing an ease in the intercalation of polymers.<sup>10–14</sup>

The production of organically modified organoclays by exchange of intragallery cations with alkylammonium ions has received great interest in the last decade.<sup>15</sup> The main problem with ammonium organoclays is the low thermal stability that they exhibit during processing of polymer nanocomposites at temperatures above 200°C; for example, in the melt processing of polyamides (PA6, PA66) and poly (ethylene terephthalate)

Additional Supporting Information may be found in the online version of this article.

© 2012 Wiley Periodicals, Inc.

(PET). Thermal degradation during processing can initiate or catalyze polymer degradation, and lead to a variety of undesirable effects during processing and in the final product.<sup>16,17</sup> Surface energy, basal spacing, and thermal stability of these organoclays depend strongly on the chemical structure, packing density, the type of cation existing in the surfactant and the degree of cation exchange. Because the processing stability of polymer nanocomposites is highly influenced by the thermal stability of both the polymer and the organoclay, efforts have been made to synthesize thermally stable organoclays based on stibonium, phosphonium, or imidazolium surfactants. The phosphonium surfactants incorporate mainly short alkyl chains, phenyl, and usually a long alkyl chain. These organoclays exhibit substantially higher thermal stability than ammonium surfactant modified organoclays. Phosphonium compounds also enhance flame retardance.<sup>18,19</sup> In addition, phosphonium salts are capable of undergoing a wider range of reactions and behave differently than their ammonium counterparts owing to the greater steric tolerance of the phosphorus atom in phosphonium salts and the participation of its low-lying *d*-orbitals in the processes of making and breaking chemical bonds.<sup>18</sup>

Polyester-based nanocomposites are considered as novel materials with promising properties for packaging applications. PET nanocomposites are often prepared at elevated processing temperatures above 280°C. Because the thermal stability of organoclays with alkyl-ammonium cations has caused severe problems during processing of PET, the present research is directed towards the preparation of organoclays that are thermally stable at high temperatures. For instance, polyester/clay nanocomposites prepared by *in situ* polymerization result in high levels of dispersion and improved physical properties. However, a more commercially viable approach with conventional melt processing leads to poorly dispersed clay in the polymer matrix. This phenomenon is attributed to the low decomposition temperature (250°C) of the ammonium salt modifier bound to the clay surface.

Poly(ethylene terephthalate) (PET) is a thermoplastic polyester with poor impact resistance and high notch sensitivity. Furthermore, in PET/clay nanocomposites, addition of clay may impart brittleness to the resulting material. This can be overcome by dispersing elastomeric polymers into the polymeric matrix.<sup>20</sup> In addition, the presence of thermally stable organoclay can overcome the problem of melt compounding and processing at high temperatures.<sup>19</sup>

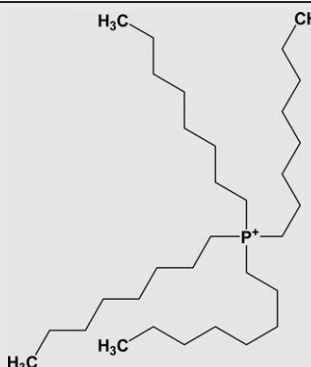
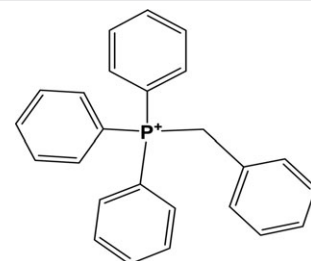
The present study is aimed at exploring the purification and modification of montmorillonite rich bentonites by organic salts with high thermal stability. The study is also focused on the effects of using these modified organoclays on the morphology, melt flow, mechanical, and thermal properties of PET based nanocomposites with and without an elastomeric compatibilizer.

## EXPERIMENTAL

### Materials

The sodium montmorillonite rich bentonite clay (KAR-BEN) used in this study was mined from Resadiye/Tokat region in Turkey and supplied by Karakaya Bentonit (Turkey). The raw

**Table I.** Chemical Structure of the Surfactants

Surfactant	Cation	Anion
Tetraoctyl phosphonium bromide; TO-P Br; (MW: 563. 76 g mol <sup>-1</sup> )		Br <sup>-</sup>
Benzyltriphenyl phosphonium chloride; BZLTP-P Cl; (MW: 388. 87 g mol <sup>-1</sup> )		Cl <sup>-</sup>

(unpurified) bentonite clay (B) contained 90% montmorillonite as reported by the supplier. Phosphonium salts were purchased from Aldrich Company (Munich, Germany). Their names, structures and properties are given in Table I. Phosphonium surfactants with different chain groups (alkyl and aryl) attached to the phosphonium cation were used in the modification of the purified bentonites. These were tetraoctyl phosphonium bromide (TO-P Br) and benzyl triphenyl phosphonium chloride (BZLTP-P Cl).

Poly(ethylene terephthalate) with an intrinsic viscosity of 0.57 dL g<sup>-1</sup> was purchased from ADVANSA Company, Adana, Turkey. Lotader® AX8900 resin (a random terpolymer of ethylene, methyl acrylate, and glycidyl methacrylate (E-MA-GMA)) was purchased in pellet form from Arkema, (Colombes, France) and used as an impact modifier/compatibilizer for PET. The epoxy functionality of GMA can react with the carboxyl and hydroxyl end groups of PET in the melt phase to form a graft copolymer.<sup>21</sup> Hence, the functionalized polymer E-MA-GMA can also function as a compatibilizer.

### Preparation of Organoclays

Prior to organic surface modification, the raw bentonite clay was purified via sedimentation according to the procedure discussed earlier<sup>22</sup> to obtain highly pure montmorillonite by removing non-clay and other clay minerals. To prepare phosphonium-treated purified bentonites; the purified bentonite (PB) was initially dried in vacuum at 120°C for 12 h. The amount of the surfactants added to all the clays was 1.1 times the CEC (cation exchange capacity). Purified clay (10 g) was

put into 1 L of distilled water at room temperature in a glass beaker equipped with a mechanical stirring bar. After 24 h, mixing was stopped and the system was heated until it reached 80°C. A solution of ethyl alcohol (400 mL) containing the surfactant, at 1.1 times the CEC, was poured into the clay dispersion. Mixing was continued for 2 h at 80°C, and then the organoclay was filtered and washed with hot water (80°C) using coarse Whatman filter paper. Washing was repeated for at least three times, until no halide traces were detected with silver nitrate. After washing, the organoclay was dried overnight at room temperature, followed by drying at 120°C for 24 h under vacuum. It was then ground in a mortar (<106 μm) and dried again under the same conditions and stored in a desiccator. Tetraoctyl phosphonium organoclays were greasy due to the insolubility of the salt itself, and thus they could not be sieved to sizes <150 μm.

### Preparation of PET Nanocomposites

**Processing.** PET based nanocomposites were prepared in air atmosphere by melt compounding using a corotating, intermeshing Thermoprism TSE 16 TC twin screw extruder with an *L/D* ratio of 24 (*L* = 384 mm, *D* = 16 mm). PET/elastomer blend, PET/organoclay binary nanocomposites and PET/organoclay/elastomer ternary nanocomposites were prepared for comparison purposes. Optimum amounts of organoclay and elastomer to balance the stiffness and toughness of the materials were found to be 2 and 5 wt %, respectively. During the experiments, the feed rate, screw speed, and the temperature profiles were kept constant for PET at 25 g min<sup>-1</sup>, 350 rpm, and 200–275–275–280°C from the main hopper to the die, respectively.

Pure PET, PET/elastomer blend, and binary and ternary PET nanocomposites were extruded twice to increase the duration of mixing. Drying was performed under vacuum for 24 h at 120°C for the organoclays and for 12 h at 40°C for the elastomers. Drying step was repeated before each processing step, since the presence of even small traces of moisture can cause significant hydrolytic degradation of PET.

The specimens were injection molded by a DSM Xplore laboratory scale micro injection molding equipment. During the molding process, the barrel temperature was adjusted to 275°C and the mold temperature was set to 21°C. All injected molded samples were dried for 24 h under vacuum in a desiccator prior to analysis.

### Morphology and Clay Dispersion

X-ray diffraction (XRD) was used to investigate the morphology of the purified clay, modified organoclays, and the produced nanocomposites. The basal distance in the organoclays and in the PET/organoclay nanocomposites was determined using a RIGAKU D/MAX 2200/PC X-ray diffractometer, that generated a voltage of 40 kV and a current of 40 mA from monochromatic Cu K $\alpha$  radiation source ( $\lambda$  = 1.5418 Å). The diffraction angle 2 $\theta$  was scanned from 1° to 10° for the polymers (using dog bone shaped tensile bars) and from 1° to 40° for the clays at a scanning rate of 2° per minute and a step size of 0.02°. To calculate the distance between the silicate layers, Bragg's law was used.

Clay dispersion was observed by transmission electron microscopy (TEM). Sections of 70 nm in thickness were cryogenically cut with a diamond knife at a temperature of -100°C from polymer/organoclay binary and polymer/organoclay/elastomer ternary nanocomposites. All of the samples were trimmed parallel to the molding direction, and examined by a Tecnai™ G2 F30 transmission electron microscope at an acceleration voltage of 120 kV.

### Failure Mechanism and Elastomer Dispersion

To examine the failure mechanism and elastomer dispersion, the impact-fractured surfaces of the nanocomposites were scanned by a low voltage JEOL JSM-6400 scanning electron microscope (SEM). Nanocomposites containing elastomers were etched with boiling xylene for 6 h to extract the elastomeric phase.

### Melt Flow Properties

Melt flow index (MFI) measurements were carried out using an omega melt flow indexer. Because melt flow index values are inversely related to the melt viscosity, changes in viscosity values were evaluated for each formulation. Conditions of temperature and load were selected as 260°C and 2.16 kg for PET (ASTM D1238-79), and are in accordance with the material specifications. It is also important to note that a more common test for PET is the intrinsic viscosity; however this method was not performed due to the presence of the clay particles.

### Mechanical Properties

Tensile tests were performed by using a Shimadzu Universal testing machine AG-IS (100kN) and percent elongation at break were determined from the stress–strain curves. Charpy impact strength of notched specimens with the dimensions of 80 × 10 × 4 mm<sup>3</sup> was measured by using a pendulum Ceast Resil Impactor. All mechanical tests were performed at 23°C ± 2°C, and the averages of five test results are reported.

### Thermal Properties

Thermal gravimetric analysis (TGA) was performed by a Shimadzu DTG-60H thermal analyzer under ultrahigh purity nitrogen atmosphere. The scanning rate used was 15°C min<sup>-1</sup> for the clay, organoclays and nanocomposites.

Differential scanning calorimetry (DSC) measurements were carried out under nitrogen atmosphere by using DSC-60 Shimadzu differential scanning calorimeter, to evaluate the changes in melting temperature (*T<sub>m</sub>*) and percent crystallinity due to the presence of impact modifiers and organoclays in PET. Samples (~6.5 mg) were cut from dry tensile bars and scanned from 25 to 300°C at a heating rate of 10°C min<sup>-1</sup>. Percent crystallinity was calculated by using the heat of fusion of the specimen. The heat of fusion for 100% crystalline PET was taken as 135.98 J g<sup>-1</sup>.<sup>23</sup>

## RESULTS AND DISCUSSION

### Morphology and Clay Dispersion

The XRD diffraction patterns of the raw clay bentonite (B), purified bentonite (PB) and purified bentonite modified with phosphonium salts S (PB.S) used in this study were obtained. XRD patterns of the clays and organoclays are shown in Figure 1.

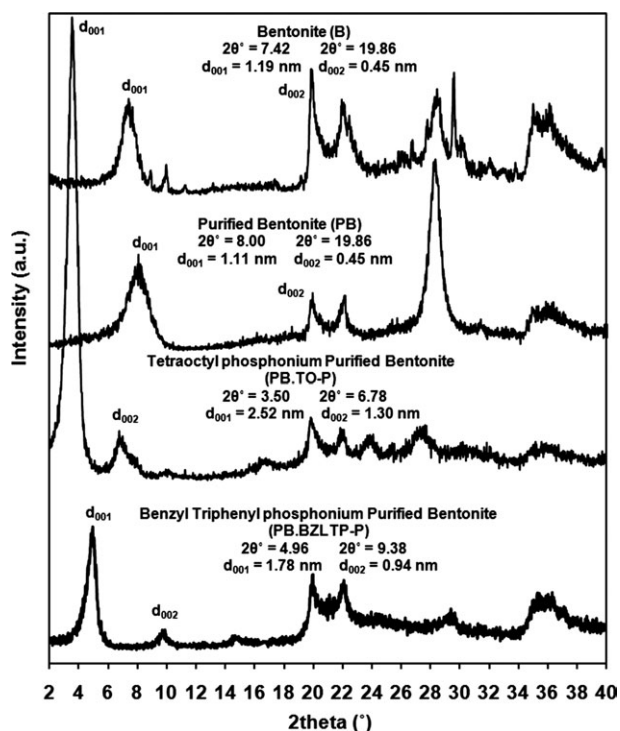


**Figure 1.** XRD patterns of bentonite (B), purified bentonite (PB) unmodified and modified by TO-P Br salt (PB.TO-P) and BZLTP-P Cl salt (PB.BZLTP-P).

The XRD results show that the raw (unpurified) clay mainly consisted of montmorillonite with nonclay mineral impurities such as analcime, calcite, clinoptilolite, dolomite, feldspar, quartz, Illite, opal-C, and  $\alpha$ -cristobalite. After purification, negligible amounts of quartz and  $\alpha$ -cristobalite were present. Purified bentonite had an interlayer spacing of 1.11 nm compared to 1.19 nm for the raw bentonite, and this can be attributed to the elimination of a portion of the monomolecular water layer between the montmorillonite layers.<sup>17</sup>

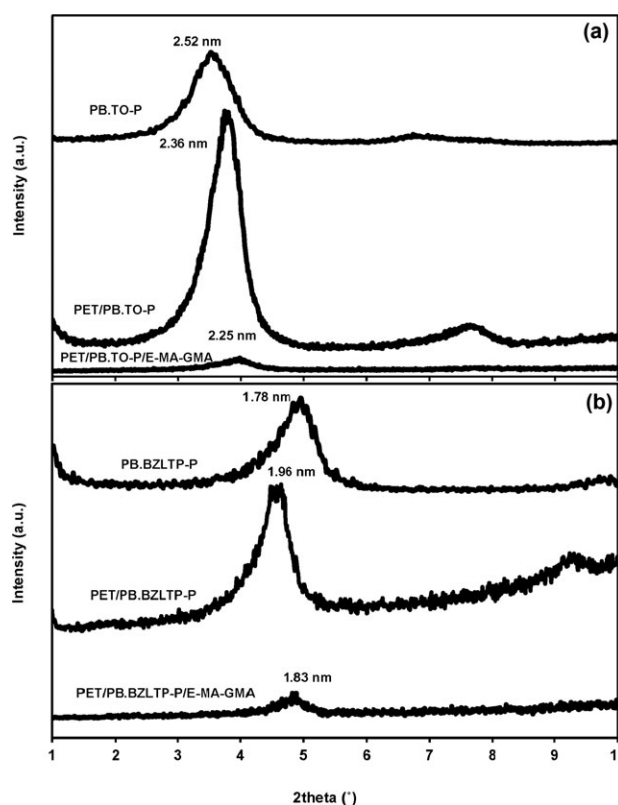
The *d*-spacings of clay, organoclays, PET-based binary and ternary nanocomposites are indicated in Figures 1 and 2. The basal spacing of purified clay increased upon ion exchange with the TO-P Br and BZLTP-P Cl salts, from 1.11 to 2.52 nm and 1.78 nm, respectively. The high molecular weight surfactant (TO-P Br with long alkyl chains) produced organoclays with a higher basal spacing (2.52 nm) indicating an arrangement that is in between pseudo-trilayer arrangement and paraffin-type of alkyl chains. The low molecular weight surfactant (BZLTP-P Cl with the phenyl groups) led to a smaller basal spacing (1.78 nm) corresponding to a bilayer arrangement of chains.<sup>19,24</sup>

XRD patterns for (PB.TO-P) and the PET-based binary and ternary nanocomposites with PB.TO-P and E-MA-GMA are shown in Figure 2(a). The XRD patterns of these nanocomposites revealed a slight decrease in the basal distance from 2.52 to 2.36 nm for the binary nanocomposite and 2.25 nm for the ternary nanocomposite. The reduction in the *d*-spacing after melting and cooling of organomodified bentonite has been attributed to crystallization of the polymer that occurs during cooling

following extrusion<sup>17</sup> or high temperature oxidative degradation. The cocrystallization of PET chains with the ethylene units of the intercalant and compatibilizer could also cause such reduction. Another explanation is the evaporation of the organic salt while drying the organoclay. A third possible argument is that the high pressure in injection molding causes the clay layers to collapse. Probably, either one or a combination of these mechanisms took place.

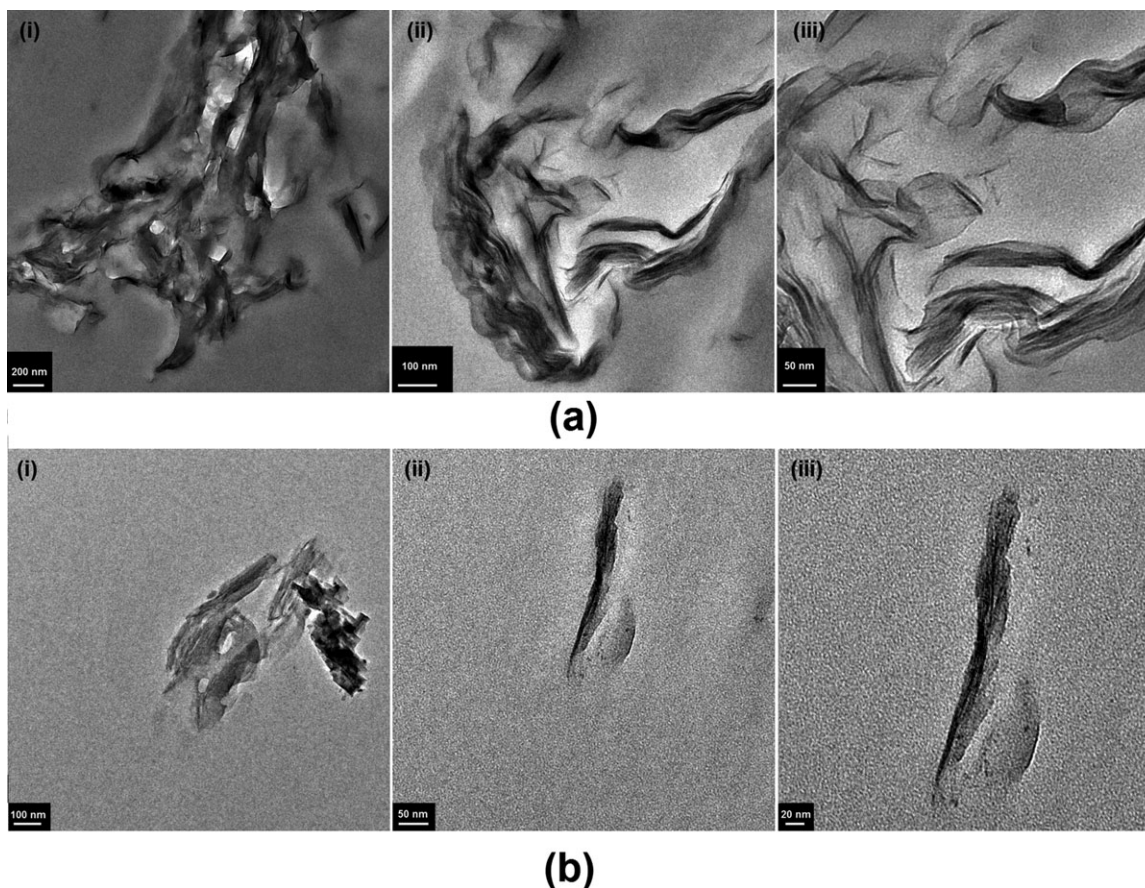
XRD patterns for (PB.BZLTP-P) and the PET binary and ternary nanocomposites with PB.BZLTP-P and E-MA-GMA are shown in Figure 2(b). The XRD patterns of these nanocomposites revealed a slight increase in the basal distance from 1.78 to 1.96 nm for the binary nanocomposite and to 1.83 nm for the ternary nanocomposite with E-MA-GMA. The slight enhancement in the basal spacing of PB.BZLTP-P organoclay after compounding with PET does not imply delamination, and TEM micrographs would give a better explanation of the structure of the composite.

Figure 3(a,b) shows the TEM images of PET/PB.TO-P/E-MA-GMA and PET/PB.BZLTP-P/E-MA-GMA ternary nanocomposites, respectively at different magnifications. In general, the behavior of the organoclays in composites is mainly attributed to the initial basal spacing of the organoclay. In our study, the intercalation of PB.TO-P layers is clear through their dispersion in the E-MA-GMA elastomeric phase. In fact, PB.TO-P organoclay is expected to exhibit good miscibility with PET owing to



**Figure 2.** XRD patterns of (a) PB.TO-P, PET/PB.TO-P and PET/PB.TO-P/E-MA-GMA and (b) PB.BZLTP-P, PET/PB.BZLTP-P and PET/PB.BZLTP-P/E-MA-GMA.





**Figure 3.** TEM micrographs of (a) PET/PB.TO-P/E-MA-GMA ternary nanocomposite: (i) 200 nm, (ii) 100 nm, (iii) 50 nm and (b) PET/PB.BZLTP-P/E-MA-GMA ternary nanocomposite: (i) 100 nm, (ii) 50 nm, (iii) 20 nm.

the paraffin-type arrangement of the layers in PB.TO-P organoclay prior to compounding. This is considered as the main factor for the polymer chains to penetrate easily between the clay layers. However, PB.BZLTP-P exhibits weak dispersion and presents more agglomerates but it is still partially intercalated, although the presence of aromatic groups in PB.BZLTP-P organoclay may be expected to promote compatibility with PET, since it contains aromatic groups. Thus, PB.TO-P and PB.BZLTP-P organoclays resulted in intercalated and partially intercalated nanocomposites, respectively.

#### Failure Mechanism and Elastomer Dispersion

The SEM micrographs of the PET, PET/E-MA-GMA blend and PET binary and ternary nanocomposites are shown in Figure 4. The average domain size and the impact strength of the materials are listed in Table II. In the SEM micrograph of PET shown in Figure 4(a), the straight crack lines and smoothness indicate the brittle structure of PET that has low impact strength. The featureless structure of pure PET disappears and tortuous propagation lines appear when PET is melt blended with E-MA-GMA [Figure 4(b)], and this can be clearly noticed in the significant increase in the impact strength of PET ( $2.9 \text{ kJ m}^{-2}$ ) to  $4.8 \text{ kJ m}^{-2}$  for the PET/E-MA-GMA blend. This improvement in the toughness of PET/E-MA-GMA blend is attributed to the optimum adhesion between PET and E-MA-GMA resulting from the

intermolecular reactions between the two polymers. If the adhesion is low between the polymer and the elastomer, the cavitation mechanism can not take place, and the impact strength would be low. E-MA-GMA is a functionalized polymer used as a compatibilizer in which the epoxy functionality of GMA reacts with the carboxyl and hydroxyl end groups of PET in the melt phase to form a graft copolymer.<sup>21</sup> E-MA-GMA reduces the effective area bearing the tensile load and creates cavitation which is a major mechanism of the stress relief in impact.

PET/organoclay binary nanocomposites exhibit high interfacial interactions as observed in Figure 4(c,d). The SEM micrographs of the PET/organoclay/E-MA-GMA ternary nanocomposites are shown in Figure 4(e–f). When cavitation and extensive deformation of the matrix occur, the blend becomes tougher.<sup>25</sup> SEM micrographs taken at  $250\times$  magnification show that cracks propagate along more tortuous paths in all the nanocomposites compared to pure PET explaining the improvement in the toughness results.

When compared to average domain size of the elastomeric phase in the PET/E-MA-GMA binary blend, that has an average diameter of 205.0 nm, the incorporation of PB.TO-P in PET/PB.TO-P/E-MA-GMA ternary nanocomposite decreased the domain size to 192.2 nm owing to the changes in melt flow index properties and the barrier effect of the well dispersed PB.TO-P

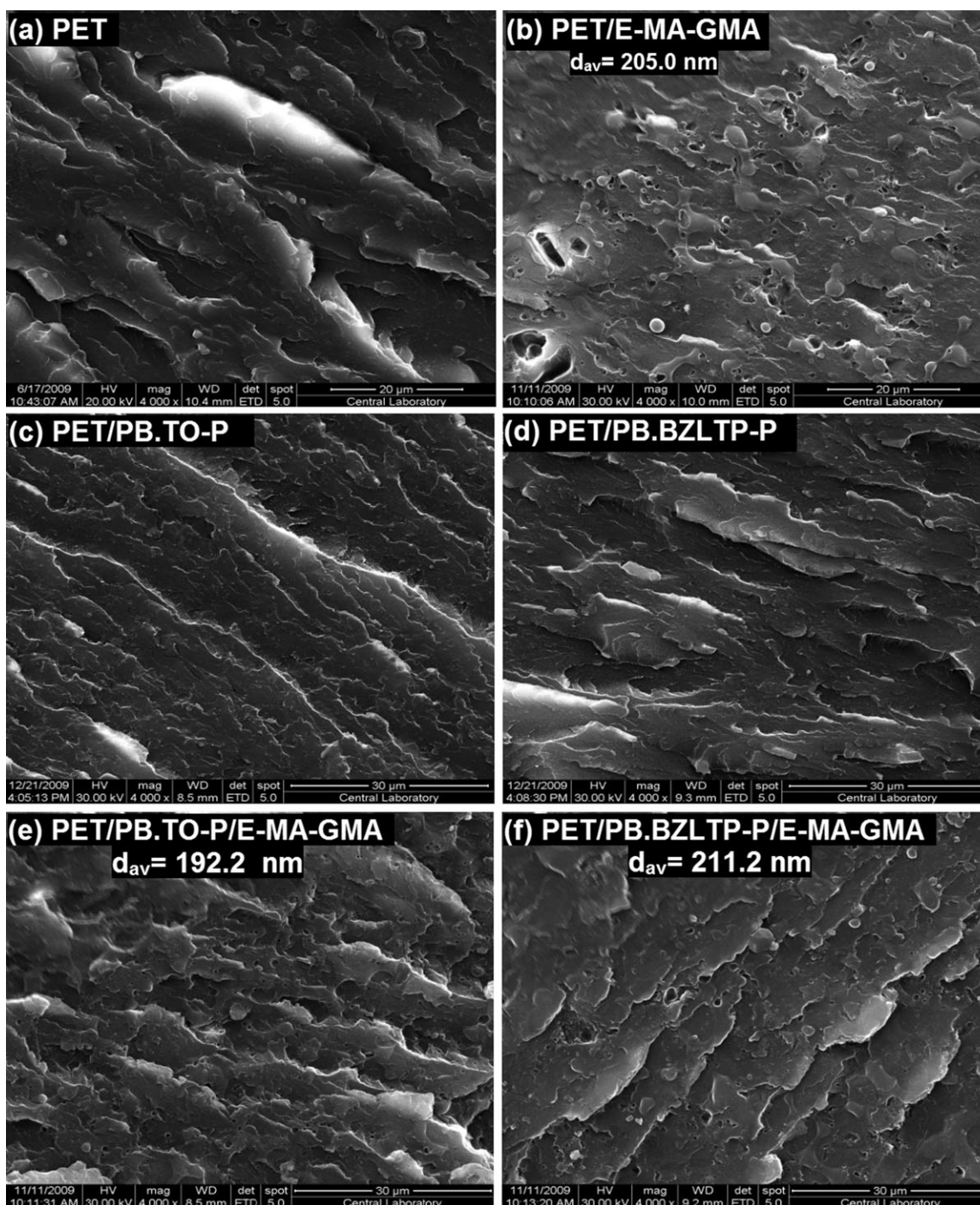


Figure 4. SEM micrographs of the PET based compositions.

organoclay, that prevents coalescence of the elastomeric domains. TEM micrographs shown in Figure 3(a) confirm the well dispersion of PB.TO-P in the ternary nanocomposite.

The poor dispersion of PB.BZLTP-P organoclay resulted in the lowest toughness among all the nanocomposites. The toughness of PET/PB.BZLTP-P/E-MA-GMA ( $3.4 \text{ kJ m}^{-2}$ ) is lower compared to that of PET/E-MA-GMA blend ( $4.8 \text{ kJ m}^{-2}$ ). The elastomer domain size in PET/PB.BZLTP-P/E-MA-GMA is higher than that in PET/E-MA-GMA, since PB.BZLTP-P exhibits low

dispersion, and most probably the silicate layers reside mostly at the interphase between PET and the elastomer.

#### Melt Flow Properties

Melt flow index values of PET compositions are given in Table III. The melt viscosity of PET decreased significantly (MFI increased) after extrusion twice due to degradation and chain scission of the polymer. In this case, the molecular bond usually breaks shortening the overall chain.<sup>20</sup>



**Table II.** Average Domain Size and Impact Strength of the PET-Based Samples

Composition	$d_{av}^a$ (nm)	Impact strength ( $\text{kJ m}^{-2}$ )
PET (extruded twice)	-	2.9
PET/E-MA-GMA	205.0	4.8
PET/PB.TO-P/E-MA-GMA	192.2	4.7
PET/PB.BZLTP-P/E-MA-GMA	211.2	3.2

<sup>a</sup>Average domain size.

The MFI of PET is much higher than that of E-MA-GMA under the same conditions. The epoxy functionality of GMA reacted with PET and formed a viscous PET/E-MA-GMA blend and resulted in lower MFI than PET has.

The concentration of the clays incorporated into the PET/organoclay binary nanocomposites is the same (2 wt %). Thus, the structure and size of organoclay particles and their compatibility with PET are the main factors for the effects of the fillers. In binary PET/organoclay nanocomposites, due to the filler effect, the addition of organoclay decreased the MFI (increased the viscosity) compared to the PET that was extruded twice. The compatibility between the polymer matrix and the surfactant residing at the surface of organoclay and the gallery distance of the organoclays are crucial to interpret the melt flow behavior of the nanocomposites.<sup>26,27</sup> The incorporation of elastomer to the binary nanocomposites to produce ternary nanocomposites decreased the MFI, owing to the low MFI of the elastomer, as well as the reaction between the epoxy functionality of GMA and PET.

### Mechanical Properties

The tensile properties of the PET, PET blend, PET binary and ternary nanocomposites are shown in Table IV. The choice of the elastomer and its concentration are the main factors in preparing nanocomposites with optimum properties. Pure E-MA-GMA is reported to have strain at break of 1100 %, and it is a suitable elastomer to be used with PET owing to its functional groups and epoxy functionality that can react with the carboxyl and hydroxyl end groups of PET in the melt phase to form a chain-extended graft copolymer. The concentration of the elastomer E-MA-GMA was chosen as 5 wt % owing to the balanced stiffness vs. impact strength properties that it imparts based on an optimization work done in an earlier study.<sup>20</sup>

**Table IV.** Mechanical Properties of the PET-Based Compositions

Composition	Tensile strength (MPa)	Young's modulus (GPa)	Elongation at break (%)	Impact strength ( $\text{kJ m}^{-2}$ )
PET (extruded twice)	52.5 ± 0.3	1.75 ± 0.05	3.9 ± 0.3	2.9 ± 0.2
PET/E-MA-GMA	50.4 ± 0.4	1.67 ± 0.03	208.7 ± 4.7	4.8 ± 0.5
PET/PB.TO-P	56.9 ± 0.8	1.96 ± 0.01	123.7 ± 22.2	3.1 ± 0.1
PET/PB.BZLTP-P	56.1 ± 4.3	2.15 ± 0.05	2.4 ± 0.3	3.2 ± 0.2
PET/PB.TO-P/E-MA-GMA	49.6 ± 0.5	1.64 ± 0.02	96.4 ± 2.1	4.7 ± 0.1
PET/PB.BZLTP-P/E-MA-GMA	46.1 ± 1.1	1.64 ± 0.01	4.4 ± 0.2	3.4 ± 0.7

**Table III.** MFI Results of the PET-Based Compositions

Composition	MFI (g/10 min)
PET (not extruded)	357.5 ± 18.7
PET (extruded twice)	486.8 ± 31.2
E-MA-GMA	7.0 ± 0.7
PET/E-MA-GMA	187.3 ± 5.1
PET/PB.TO-P	420.2 ± 12.0
PET/PB.BZLTP-P	423.4 ± 9.5
PET/PB.TO-P/E-MA-GMA	240.4 ± 16.3
PET/PB.BZLTP-P/E-MA-GMA	250.2 ± 9.8

The addition of elastomer to PET decreased the tensile strength and Young's modulus of PET owing to the low tensile strength and modulus of the elastomer. However, the addition of organoclay to PET resulted in an increase in the tensile strength and Young's modulus owing to the strength and stiffness of the organoclays.<sup>28</sup> The high aspect ratio of the organoclays promotes these effects. The aryl phosphonium PB.BZLTP-P organoclay exhibited a decrease in tensile strength (46.1 MPa) compared to pure PET (52.5 MPa) due to the poor dispersion of BZLTP-P organoclay in the ternary nanocomposites, as mentioned earlier.

The addition of E-MA-GMA elastomer to PET resulted in considerable ductility, and neck propagation formed along the gauge section of the tensile test samples before they broke. The elongation at break of PET/PB.TO-P binary nanocomposite (123.7%) decreased upon addition of E-MA-GMA to produce PET/PB.TO-P/E-MA-GMA ternary nanocomposite (96.4%). This decrease could be attributed to the reinforcing effect of clay in the elastomeric region of the ternary nanocomposite. However, elongation at break of PET/PB.BZLTP-P binary nanocomposite (2.4%) and of PET/PB.BZLTP-P/E-MA-GMA ternary nanocomposite (4.4%) is comparable to that of pure PET. The ductility of PET/PB.TO-P binary nanocomposites can be attributed to the better dispersion of the PB.TO-P organoclay in the PET matrix, whereas the poor dispersion of PB.BZLTP-P resulted in brittleness as well as low tensile strength.

Impact strength of PET, PET blend and PET based nanocomposites is given in Table IV. Impact strength of PET/E-MA-GMA blend increased from 2.9  $\text{kJ m}^{-2}$  for pure PET to 4.8  $\text{kJ m}^{-2}$  in PET/E-MA-GMA owing to the cavitation mechanism

**Table V.** Thermal Decomposition Results of the Clays, Salts, and Organoclays

Material	$T_{\text{onset}}^a$ (°C)	Mass loss at $T_{\text{onset}}$ (%)	Mass loss at 275°C (%)	Decomposition temperature at 2% mass loss (°C)	Decomposition temperature at 5% mass loss (°C)	$T_{\text{max. D.R.}}^b$ (°C)
<b>Clay</b>						
B	628	3.00	1.90	299	666	689
PB	653	2.42	1.31	533	769	728
<b>Salt</b>						
TO-P Br	360	2.3	0.66	302	329	387
BZLTP-P Cl	340	0.1	0.00	338	339	345
<b>Nanoclay</b>						
PB.TO-P	327	0.88	1.45	290	338	513
PB.BZLTP-P	354	2.75	1.95	284	380	474

<sup>a</sup> $T_{\text{onset}}$ : Temperature corresponding to the cross-section of the two tangents around the main degradation point in TGA thermogram, <sup>b</sup> $T_{\text{max. D.R.}}$ : Temperature at maximum Decomposition rate.

introduced by the elastomeric domains. The addition of organoclay makes the crack propagation paths more tortuous as observed by SEM owing to the interaction between the matrix and clay surface, thus the toughness increased also by the addition of organoclays to PET. In PET ternary nanocomposites, PB.TO-P-based ternary nanocomposites exhibited an impact strength value  $4.7 \text{ kJ m}^{-2}$  which is higher than that of PB.BZLTP-P-based ternary nanocomposite that exhibited a lower value of  $3.4 \text{ kJ m}^{-2}$ . This is due to the better dispersion of alkyl phosphonium organoclay (PB.TO-P) compared to aryl phosphonium organoclay (PB.BZLTP-P) within the PET matrix. In addition, the presence of rigid aromatic groups in PB.BZLTP-P may lead to lower impact strength of PET/PB.BZLTP-P/E-MA-GMA ternary nanocomposite.

### Thermal Analysis

**Thermogravimetric Analyses of Surfactants, Clays, and Organoclays.** The thermogravimetric analyses of surfactants, clays, phosphonium organoclays and PET nanocomposites were carried out under nitrogen atmosphere to investigate the effects of salts used on the clay and the resulting nanocomposites. The results are reported in Tables V and VI in terms of onset decomposition temperature and peak decomposition temperature using the thermograms shown in Figures 5–7.

The higher onset decomposition temperature of the alkyl phosphonium salt (onset decomposition temperature of 360°C with 2.3% mass loss) can be attributed to its higher molecular weight compared to the aryl phosphonium salt (onset decomposition temperature of 340°C with 0.1% mass loss). Also, the temperature at maximum decomposition rate is 387°C for TO-P Br and 345°C for BZLTP-P Cl. At 275°C, BZLTP-P Cl surfactant exhibited no mass loss, whereas TO-P Br exhibited 0.66% mass loss. Thus, both phosphonium surfactants exhibited the desirable thermal stability for polymer processing temperatures in the range of 200–300°C.

The thermal stability of the clay, along with the cation exchange capacity, is negatively affected by the presence of impurities. The thermograms in Figure 5 show that the thermal stability of the bentonite clay increased significantly (~5% less weight loss) after purification owing to the discharge of undesirable inorganic minerals. The onset decomposition temperatures for B and PB are 628°C (at 3.0% mass loss) and 653°C (at 2.42% mass loss), respectively. These results confirm the importance of purification of the raw bentonites before the ion exchange process.

After the intercalation of purified bentonite with phosphonium salts, the organoclays formed also exhibited high thermal stability. The onset decomposition temperatures for PB.TO-P

**Table VI.** Thermal Decomposition Results of the PET-Based Compositions

Composition	$T_{\text{onset}}^a$ (°C)	Decomposition temperature at 2% mass loss (°C)	Decomposition temperature at 5% mass loss (°C)	Mass loss at 275°C (%)	Char yield at 600°C (%)
PET (extruded twice)	413	386	400	0.41	14.0
PET/E-MA-GMA	412	391	401	0.10	12.6
PET/PB.TO-P	420	345	396	1.92	8.2
PET/PB.BZLTP-P	424	395	409	0.29	15.9
PET/PB.TO-P/E-MA-GMA	410	382	395	0.16	11.3
PET/PB.BZLTP-P/E-MA-GMA	423	394	408	0.18	13.5

<sup>a</sup> $T_{\text{onset}}$ : Temperature corresponding to the cross-section of the two tangents around the main degradation point in TGA thermogram.



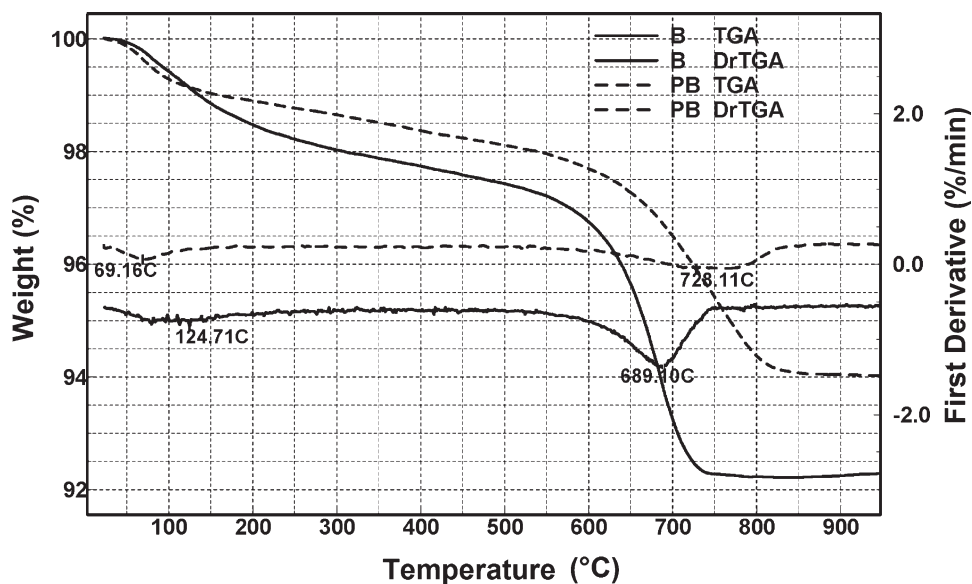


Figure 5. TGA thermograms of the bentonite (B) and purified bentonite (PB).

and PB.BZLTP-P based organoclays are 327°C (0.88% mass loss) and 354°C (2.65% mass loss), respectively (Fig. 6). The high thermal stability of both phosphonium organoclays (PB.TO-P and PB.BZLTP-P) is attributed to the crucial removal

of the halide. For the onset decomposition temperature of the salts, the molecular weight is the dominant factor, whereas considering the onset decomposition of the organoclays, the aryl-based organoclay PB.BZLTP-P exhibited higher onset

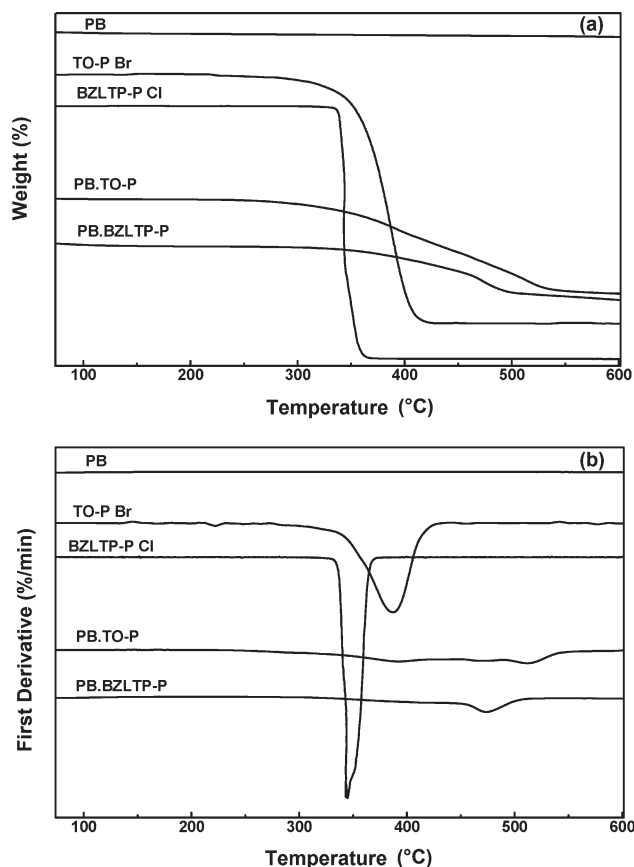


Figure 6. TGA thermograms of the purified bentonite (PB), phosphonium salts and modified organoclays.

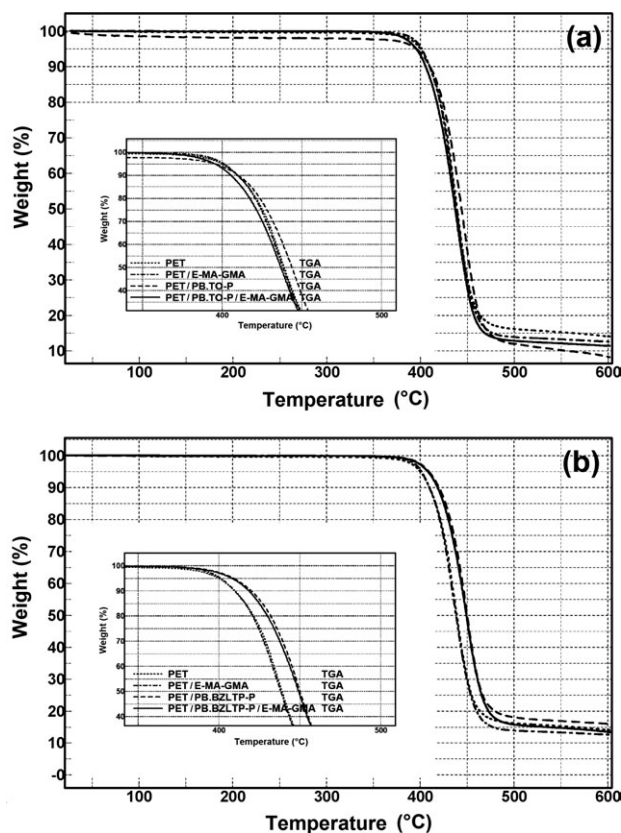


Figure 7. TGA thermograms of (a) PET, PET/E-MA-GMA, PET/PB.TO-P, and PET/PB.TO-P/E-MA-GMA (b) PET, PET/E-MA-GMA, PET/PB.BZLTP-P, and PET/PB.BZLTP-P/E-MA-GMA.

temperature than the alkyl-based PB.TO-P did. The onset decomposition temperature of both organoclays is quite higher than the processing temperature of PET matrix (275°C) used in this study. At 275°C, TO-P Br-based organoclay exhibited 1.45% mass loss, whereas BZLTP-P Cl-based organoclay exhibited 1.95% mass loss.

#### Thermogravimetric Analyses of PET Nanocomposites

The thermal decomposition data of all PET compositions taken under nitrogen atmosphere are given in Table VI. Figure 7(a,b) show the TGA graphs of PB.TO-P and PB.BZLTP-P containing nanocomposites compared to pure PET and PET/E-MA-GMA blend. It can be clearly seen that the addition of the E-MA-GMA elastomer into PET caused no significant change on the decomposition of the PET/E-MA-GMA blend. Bandyopadhyay et al.<sup>29</sup> investigated the thermal stability of PET/ammonium organoclay nanocomposites. The onset decomposition temperatures of the binary nanocomposites in nitrogen atmosphere were 10°C lower than that of pure PET. The thermal behavior of the nanocomposites in nitrogen atmosphere indicated that the addition of alkylammonium organoclays accelerated the thermal decomposition of PET matrix, which was attributed to the catalytic activity of water evolved from MMT on the degradation process. The onset decomposition temperatures for PET/PB.TO-P and PET/PB.BZLTP-P binary nanocomposites are 420 and 424°C, respectively. The thermally stable phosphonium organoclays show that the barrier effect of the silicate layers is dominant due to the formation of carbonaceous-silicate char on the surface of nanocomposites, thus in comparison to the onset decomposition temperature of PET, the onset decomposition temperature of PET/PB.TO-P and PET/PB.BZLTP-P binary nanocomposites is 7 and 11°C higher, respectively. The addition of the elastomer to produce ternary nanocomposites decreases the onset decomposition temperature. However, the values are still comparable to that of PET. PB.TO-P containing ternary nanocomposite exhibited a lower onset decomposition temperature (410°C) than PET did, whereas the onset decomposition temperature of PET/PB.BZLTP-P/E-MA-GMA ternary nanocomposite was 423°C.

#### Differential Scanning Calorimetry Results of PET Nanocomposites

Amorphous PET has poor mechanical properties, low dimensional stability and high gas permeation rate. On the other hand, crystalline PET has high strength, good dimensional stability and chemical resistance. It is widely used in the production of fibers and in carbonated beverage containers owing to its strength and low gas permeability.<sup>30</sup> The importance of crystallinity is thus vital on the properties of a composite. The effect of MMT on the crystallization behavior of PET during heating was investigated by DSC. The percent crystallinity of the PET phase is calculated as the ratio of the heat of fusion of the sample ( $\Delta H_f$ ), divided by the weight fraction of PET in the nanocomposite and the heat of fusion of the pure crystalline form of PET ( $\Delta H_f^\circ$ ). DSC thermograms of pure PET, PET/E-MA-GMA blend and binary and ternary nanocomposites were used to determine the melting point, heat of fusion and crystallinity. The thermal properties of all the materials are given in Table VII. The crystallinity of the PET in PET/E-MA-GMA

**Table VII.** Thermal Properties of the PET-Based Compositions

Composition	$T_m^a$ (°C)	$\Delta H_f^b$ (J g <sup>-1</sup> )	Crystallinity (%)
PET (extruded twice)	254.5	54.9	40.4
PET/E-MA-GMA	253.3	49.5	38.3
PET/PB.TO-P	253.0	52.6	39.5
PET/PB.BZLTP-P	252.7	55.9	41.9
PET/PB.TO-P/E-MA-GMA	256.3	43.5	34.4
PET/PB.BZLTP-P/E-MA-GMA	252.8	46.0	36.4

<sup>a</sup> $T_m$ : melting temperature, <sup>b</sup> $\Delta H_f$ : Heat of fusion.

(38.3%) is lower than that of pure PET (40.4%) implying that the elastomer interferes with the crystallinity of PET. The melting point also decreased slightly due to the dilution effect of the elastomer to PET, similar to freezing point depression. For the same reason, the crystallinity of the ternary nanocomposites is also lower than the crystallinity of the corresponding binary nanocomposites.

Organoclays are expected to act as nucleating agents in polymer based nanocomposites and increase the level of crystallinity owing to their large area that may promote heterogeneous crystallization. However, the results obtained in the present work indicate that the phosphonium based organoclays did not show significant effect as nucleating agents in the binary nanocomposites studied. The crystallinity of PET/PB.TO-P binary nanocomposite (39.5 %) decreased slightly, and PET/PB.BZLTP-P (41.9 %) binary nanocomposite increased slightly compared to the crystallinity of pure PET that was extruded twice (40.4%). Also, the melting point did not change significantly in PET/phosphonium organoclay binary nanocomposites.

## CONCLUSIONS

Thermally stable bentonites with high cation exchange capacity were produced by purification (sedimentation). The surface modification of the purified bentonite with phosphonium salts resulted in thermally stable organoclays that can be used in melt processing of high melting-point polymers such as PET. The initial basal spacing and compatibility (chain type) of the organoclay were the main factors in intercalation and dispersion of the PET/organoclay based nanocomposites. TEM results showed that the paraffin-type arrangement of the layers in PB.TO-P organoclay resulted in better dispersion in the ternary nanocomposite compared to PB.BZLTP-P organoclay did. The ternary nanocomposites produced with PB.TO-P also exhibited higher elongation at break than the nanocomposites produced with PB.BZLTP-P did. DSC results showed that the use of organoclays did not significantly promote nucleation process in PET based nanocomposites, whereas the elastomer decreased the level of crystallinity.

## ACKNOWLEDGMENTS

The authors are grateful to the Scientific and Technological Research Council of Turkey (TÜBİTAK) for their financial support and the Middle East Technical University for financially

supporting the experimental part of this research under contract number BAP-2006-07-02-00-01. Special thanks to Karakaya Bentonit A.S., Ankara, Turkey for providing the raw bentonite.

## REFERENCES

1. Xu, X.; Ding, Y.; Qian, Z.; Wang, F.; Wen, B.; Zhou, H.; Zhang, S.; Yang, M. *Polym. Degrad. Stab.* **2009**, *94*, 113.
2. Grim, R. E. *Clay Mineralogy*, 1st ed.; McGraw-Hill: New York, **1953**.
3. Liu, S.-P.; Huang, I.-J.; Chang, K.-C.; Yeh, J.-M. *J. Appl. Polym. Sci.* **2010**, *115*, 288.
4. Awad, W. H.; Beyer, G.; Benderly, D.; Ijdo, W. L.; Songtipya, P.; Jimenez-Gasco, M. M.; Manias, E.; Wilkie, C. A. *Polymer* **2009**, *50*, 1857.
5. Bergaya, F.; Theng, B. K. G.; Lagaly, G. *Developments in Clay Science: Handbook of Clay Science*; Elsevier: Amsterdam, **2006**; Vol. I.
6. Onal, M.; Sarikaya, Y.; Alemdaroglu, T.; Bozdogan, I. *Turk. J. Chem.* **2003**, *27*, 683.
7. Auerbach, S. M.; Carrado, K. A.; Dutta, P. K. *Handbook of Layered Materials*, 1st ed.; Marcel Dekker: New York, **2004**.
8. Tiwari, R. R.; Khilar, K. C.; Natarajan, U. *Appl. Clay. Sci.* **2008**, *38*, 203.
9. Tjong, S. C. *Mater. Sci. Eng.* **2006**, *53*, 73.
10. Favre, H.; Lagaly, G. J. *Clay Miner.* **1991**, *26*, 19.
11. Giannelis, E. P. *Appl. Organomet. Chem.* **1998**, *12*, 675.
12. Mert, M.; Yilmazer, U. *Adv. Polym. Technol.* **2009**, *28*, 155.
13. Isik, I.; Yilmazer, U.; Bayram, G. *Polym. Compos.* **2008**, *29*, 133.
14. Coskunes, F.; Yilmazer, U. *J. Appl. Polym. Sci.* **2011**, *120*, 3087.
15. Ray, S. S.; Okamoto, M. *Prog. Polym. Sci.* **2003**, *28*, 1539.
16. Awad, W. H.; Gilman, J. W.; Nyden, M.; Haris, R. H.; Sutto, T. E., Jr.; Callahan, J.; Truvole, P. C.; DeLong, H. C.; Fox, D. M. *Thermochim. Acta* **2004**, *409*, 3.
17. Gilman, J. W.; Awad, W. H.; Davis, R. D.; Shields, J.; Haris, R. H.; Davis, C., Jr.; Morgan, A. B.; Sutto, T. E.; Callahan, J.; Truvole, P. C.; DeLong, H. C. *Chem. Mater.* **2002**, *14*, 3776.
18. Xie, W.; Xie, R.; Pan, W.; Hunter, D.; Koene, B.; Tan, L.; Vaia, R. J. *Chem. Mater.* **2002**, *14*, 4837.
19. Calderon, J. U.; Lennox, B.; Kamal, M. R. *Appl. Clay Sci.* **2008**, *40*, 90.
20. Alyamac, E.; Yilmazer, U. *Polym. Compos.* **2007**, *28*, 251.
21. Arkema Chemicals. Available at: <http://www.arkema-inc.com/index.cfm> (accessed May **2012**).
22. Abdallah, W.; Yilmazer, U. *Thermochim. Acta* **2011**, *525*, 129.
23. Starkweather, H. W.; Zoller, P.; Jones, G. A. *J. Polym. Sci. Polym. Phys.* **2003**, *21*, 295.
24. Hedley, C. B.; Yuan, G.; Theng, B. K. G. *Appl. Clay Sci.* **2007**, *35*, 180.
25. Chapleau, N.; Huneault, M. A. *J. Appl. Polym. Sci.* **2003**, *90*, 2919.
26. Lee, K. M.; Han, C. D. *Macromolecules* **2003**, *36*, 7165.
27. Cassagnau, P. *Polymer* **2008**, *49*, 2183.
28. Seymour, R. B. *Polymer Chemistry: An Introduction*, 4th ed.; Marcel Dekker: New York, **1996**.
29. Bandyopadhyay, J.; Ray, S. S.; Bousmina, M. J. *Ind. Eng. Chem.* **2007**, *13*, 614.
30. Kong, Y.; Hay, J. N. *Polymer* **2002**, *43*, 3873.